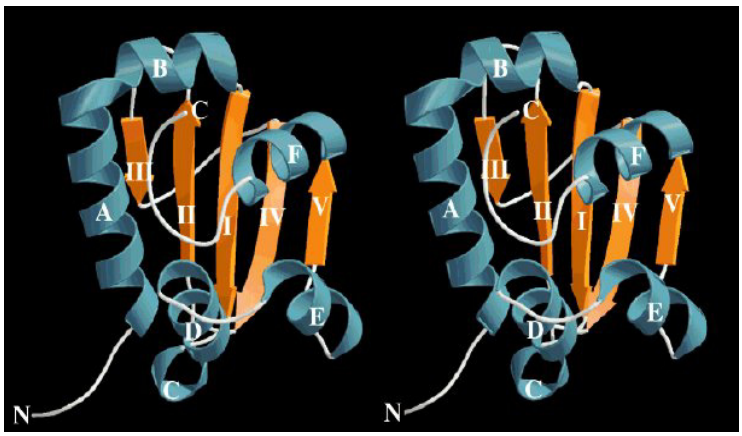

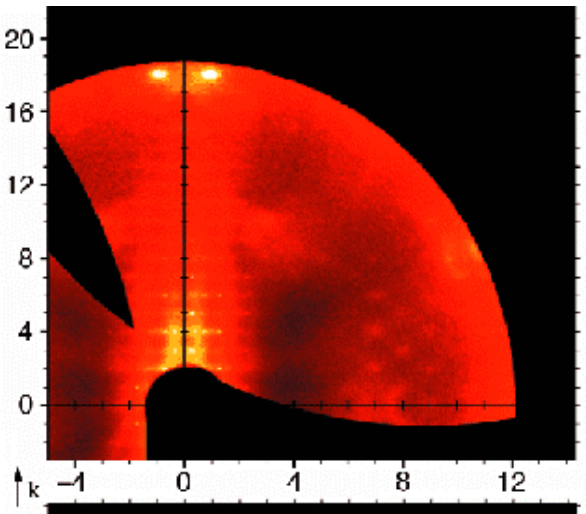

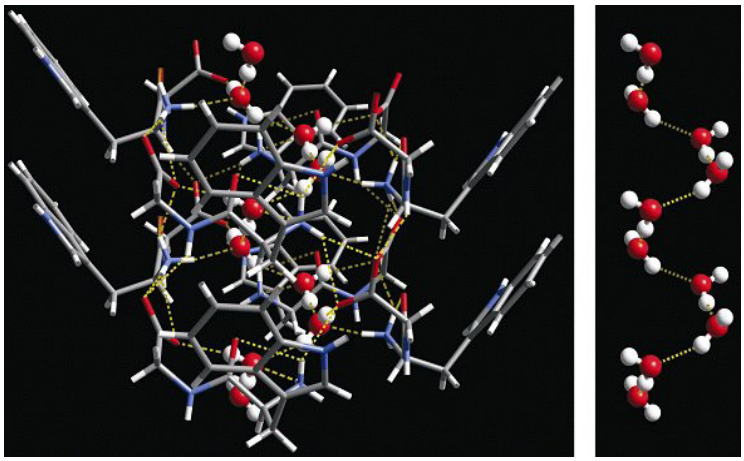

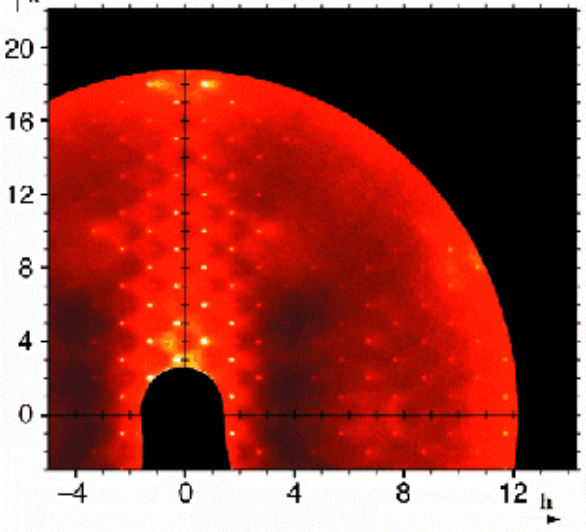

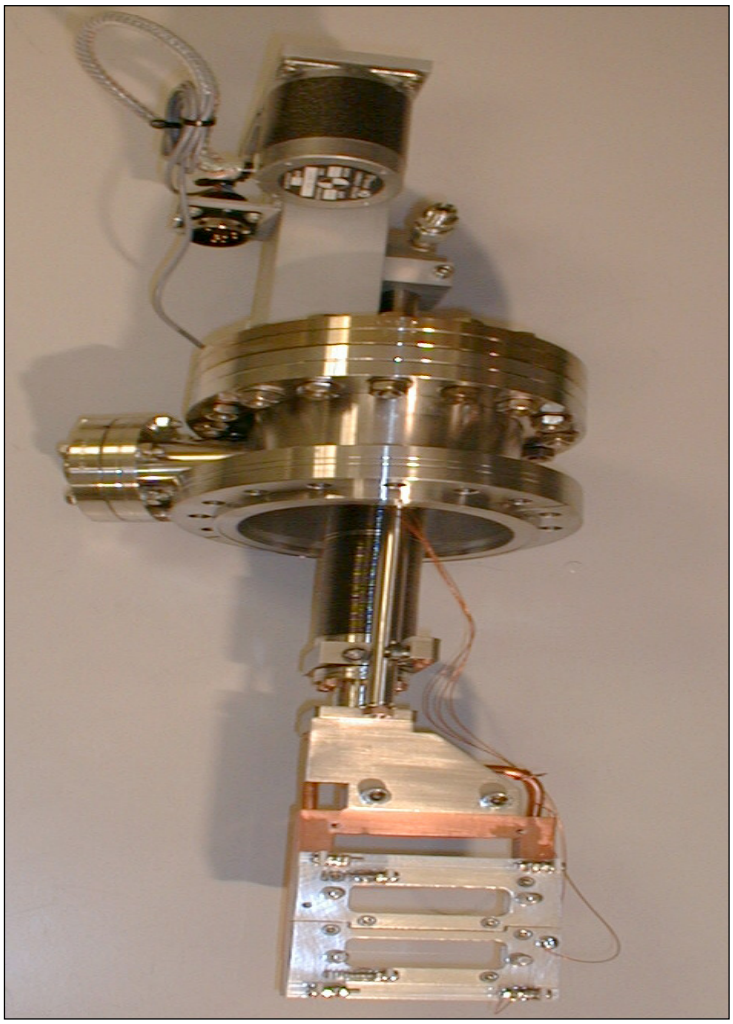

The Swiss-Norwegian Beamlines at ESRF

SNBL 2000

Annual Report:
October 1999-
September 2000

IMPRESSUM

SNBL 2000

SNBL 2000 was prepared by Weaver Unlimited for the Swiss-Norwegian Beamlines at ESRF, PO Box 220,
F-38043 Grenoble, France

SNBL Director	Hans-Peter Weber	+33 476 88 2396
SNBL Executive Assistant	Chantal Seferiadis	+33 476 88 2615
FAX		+33 476 88 2694
E-mail		ExAsst_snbl@esrf.fr
Website		www.snbl.org

May 2002

Annual Report Oct 1999- Sept 2000

CONTENTS

CONTENTS

SNBL IN BRIEF 1

The SNBL are the creation by a group of enthusiastic scientists, from both Norway and Switzerland, who had been dreaming of a synchrotron-radiation facility custom-tailored to their experimental needs.

The result is a large, user-supported facility, offering scientists from both partner countries access to specialized instruments, which are unavailable in their home laboratories, and, in some cases, not found at other synchrotron-radiation sources.

Initially conceived as a single, general purpose beamline, its design was soon modified to consist of two branch lines in order to accommodate more efficiently the large variety of experimental techniques demanded by its users.

Even though it is generally accepted nowadays that many problems in structural crystallography can be solved only with the use of synchrotron radiation, it is less widely recognized that the most challenging problems, often enough, can be puzzled out only by harnessing the combined power of two or more synchrotron-radiation based techniques (such as, e.g., powder and single-crystal diffraction). For this reason, the SNBL number four such experimental techniques, which are distributed over two beamlines, and presently include:

A. High-resolution single crystal diffractometry

B. Large-area diffraction imaging

C. High-resolution powder diffractometry

D. EXAFS spectrometry

Environmental chambers for extreme conditions (often unavailable in one's home laboratory) complement this equipment and often open up new, previously uncharted terrain.

This unusually broad range of instruments, all available in one facility, is one of the prime strength of SNBL, a one-stop facility for the solution of complex crystal structural problems.

The Swiss-Norwegian Beam Lines are located in Grenoble at the European Synchrotron Radiation Facility, next to the high-flux reactor of the Institut Laue-Langevin. This setting, together with the proximity to several universities and R&D laboratories of international high-technology companies, concur to make Grenoble a pre-eminent pole in solid-state research in Europe and provide a very stimulating working environment for users and staff of the Swiss-Norwegian Beam Lines.

FOREWORD 2

This is the third annual report of the Swiss-Norwegian Beamlines (SNBL) at ESRF, the first one having been published in 1997. Reports are issued annually, mid-year.

The annual report offers a welcome opportunity for SNBL users and staff alike to appraise what has been achieved, to learn from the past and look to the future, and to decide what ought to be done in the years to come, in short: to develop a proactive vision.

The year 2000, almost everyone forgot, was the fifth year of full operation at the SNBL. It is appropriate on this anniversary date to recall some of the more significant events that led to the SNBL:

- 1989: ESRF workshop in Frankfurt/Main. Frode Mo (Trondheim) and H-P Weber (Lausanne) meet Ch. Riekel (ESRF). Fired up by the latter's enthusiasm on the applications of synchrotron radiation, the first two decide to try to raise funds in their respective countries for a "private" beamline at ESRF.
- In 1990 UNIT (Trondheim) contributes the first NOK 2 Mio. A year later, Swiss research institutions and National Science Foundation reciprocate.
- 1992: First contract signed between Norwegian Research Council, Norwegian Users and Swiss Users Group. In the same year start of design and construction in Preston, UK.
- 1993-94: Move of optics module to Grenoble.
- 1994: First light in SNBL optics hutch.
- 1995: Begin of user operations on both beamlines.

As seen from a SNBL user's eye, the past year (1999-2000) has been a continuation of the outstandingly successful operation of both ESRF and of our own facility.

ESRF's machine (linac, synchrotron, storage ring has performed exceedingly well (96.4% reliability). Our own four experimental stations have been running according to schedule, with always two stations in operation at anyone time. Every station is not only being properly maintained, but upgrades take place continuously –subject to the availability of funds and the workload ceiling of staff.

As at other ESRF beamlines, where only minute sample volumes are often available; we have recently become interested in the use of beam condensors. We have acquired a focusing capillary, have tested it on several types of experiments, and in this yearbook we report on this new development. In parallel, we have started to develop, in-house, our own micro-focusing device. First tests have shown our concept to be very promising; the next annual report will cover this development in greater detail.

Collaboration with our larger sister facility in Switzerland, the Swiss Light Source in Villigen, is proceeding as planned and quite successfully at that, with staff being exchanged long-term and frequent short visits from both sides. Two contributions in this report illustrate the benefits of this on-going cooperation.

The success of a facility such ours depends also crucially on a steady flow of funds. At this point, I would like to take the opportunity to thank once more the backers of the Swiss-Norwegian Beam Lines at ESRF for their generous and continuing support.
Last, but not least, let me express my heart-felt gratitude to my staff for its unceasing devotion to the project. In a project such as this, the quality of the staff, more than anything else, is the key to its success.

Hans-Peter Weber, SNBL Director

Crystal structure of a complicated polar, molecular material

(Hans-Beat Buergi and Thomas Weber [Univ. Berne], Michael Estermann [ETHZ])

Crystalline materials are often built less regularly than the pictures in most textbooks would suggest. Different unit cells differ in molecular occupation, orientation or position. In spite of such disorder, or sometimes because of it, such materials may have interesting properties. Molecular inclusion compounds of the hydrocarbon host molecule perhydro-triphenylene (PHTP) with rod-shaped, polar guest molecules, *e.g.* nitrophenyl-piperazine (NPP), provide an example. Stacks of host molecules are arranged in a honeycomb architecture whose tunnels are filled with chains of guest molecules (see Fig. 1). Right- and left-handed host molecules occupy the stacks in a not-quite-random fashion. The chains of guest molecules register at different heights in different channels. Remarkably, they are all parallel, even though the channels are ~ 15 Å apart. The crystals are polar and show second harmonic generation. This material produces an extraordinarily rich diffraction pattern including Bragg peaks and incommensurate satellites, as well as diffuse streaks, planes and three-dimensional features. Almost complete patterns have been measured on beamline BM1A (SNBL) at the centre and at one tip of a prismatic crystal (298 K and 120 K).

Most of the diffuse and satellite scattering can be assigned to occupational disorder of the host, positional disorder of the guest, or to local distortions of the average structure.

Real structures are simulated with a Markov growth model.

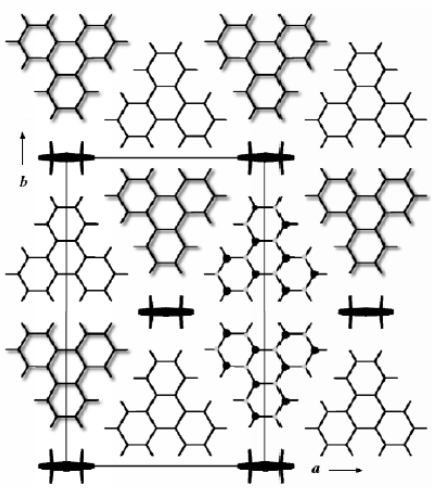

Fig. 1. The structure of $PHTP_5$.NPP viewed down the polar stacking axis of PHTP host and NPP guest molecules; z = 0.75 for shadowed PHTP molecules, z = 0.25 otherwise; z = 0, 1, 2, 3 or 4 for NPP molecules. The wavy shapes of right- and left-handed, D_3-symmetric PHTP molecules are indicated at the right margin of the unit cell. The long axis of NPP molecules is perpendicular to the plane of projection.

Its parameters are optimised with an evolutionary algorithm on 40 individuals using an R-value based on diffraction intensities as fitness criterion.

The structure simulations and Fourier transformations are calculated through a scheme of distributed computing with up to ten simultaneous processes running on PC's, SUN and SGI workstations and progressing at a rate of ~ 15 generations per day.

Fig. 2 shows a particularly interesting feature. It compares the scattering of 100 μ slabs in the centre and at a tip of the prismatic crystal.

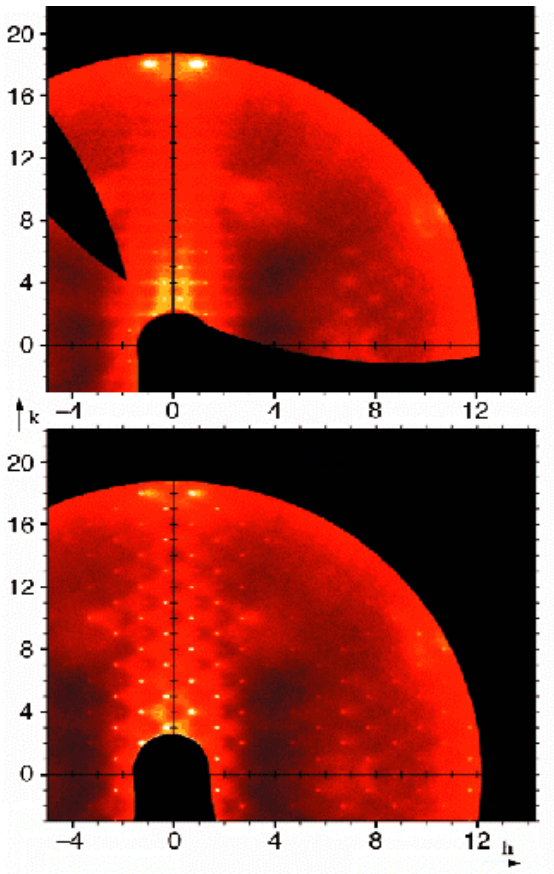

Fig. 2. hk2.4 layer from the centre (top) and a tip (bottom) of a $PHTP_5$.NPP crystal at 120 K. Note that diffuse intensities form a pseudo-rectangular pattern at the crystal centre, but are triangularly shaped at its tip.

In the center, the diffraction symmetry is nearly orthorhombic (top), whereas at the tip it is monoclinic (bottom). This implies that the crystal is not homogeneous along the stacking direction of the host and guest molecules. Note that at the crystal tip the satellite reflections are connected through triangular diffuse scattering. The former indicate a well defined long-range ordered, incommensurate modulation of the structure, the latter some dispersion of this modulation

Two conclusions emerge:

- Accurate and complete three-dimensional diffuse scattering data of a complex disordered molecular material can be measured with synchrotron radiation and three-dimensional structure models developed with a scheme of distributed computing. (The scope of such studies becomes significantly broader if the computations are parallelized).
- Diffuse scattering and thus disorder of the crystal structure along growth directions may be followed.

With an improved focusing device, spatial resolution could be significantly improved, thus providing records of the crystallisation history of disordered materials.

Principal Publication: Acta Cryst. (2001) **B57**, 1550-1556

Uni-axial negative thermal expansion in an organic crystal

(Phil Pattison [SNBL], Henrik Birkedal and Dieter Schwarzenbach [Univ. of Lausanne])

Crystal engineering has attracted increasing interest in the past few years. This subject is concerned with the design of solids with specific, controlled properties. One such property is negative thermal expansion (NTE), in which the crystal expands along one or more axes as the temperature is lowered. Several inorganic materials displaying NTE are known, but the number of organic examples is very limited. Here we present one such example, tryptophylglycine monohydrate, $TrpGly{\cdot}H_2O$, a dipeptide. The structure of this compound was solved using single crystal diffraction data

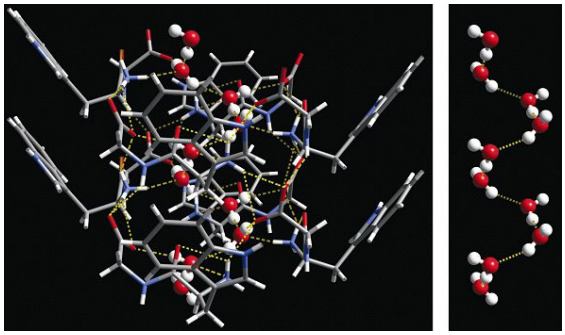

Fig. 3. Helical columns in the crystal structure of TrpGly·H_2O. The water molecules are shown by ball-and-stick while the dashed yellow lines denote hydrogen bonds. Note the columnar structure that is parallel to the c-axis.

collected at the Swiss-Norwegian Beamlines on a crystal measuring only 20x30x180 µm. Focussing optics and a MAR345 imaging-plate detector were used for the experiment. In spite of the small sample size, very high-quality data could be collected both at room temperature and 120 K.

The structure refined to very satisfying agreement factors (R_1(all) < 3.3 % at both temperatures), fully competitive with high-quality laboratory data on normal-sized samples.

The tetragonal crystal structure displays a helical assembly of peptide molecules connected through extensive hydrogen bonding (see Fig. 3). This peptide helix encloses a water helix, which is linked to the peptide framework by hydrogen bonds. The water helix is partially ordered at both temperatures with one preferred site. The occupancy of this site increases upon lowering the temperature, but has not reached full occupation at 120 K. The thermal expansion was investigated using powder diffraction and the same imaging plate detector. This method allows for rapid characterisation of phase transitions

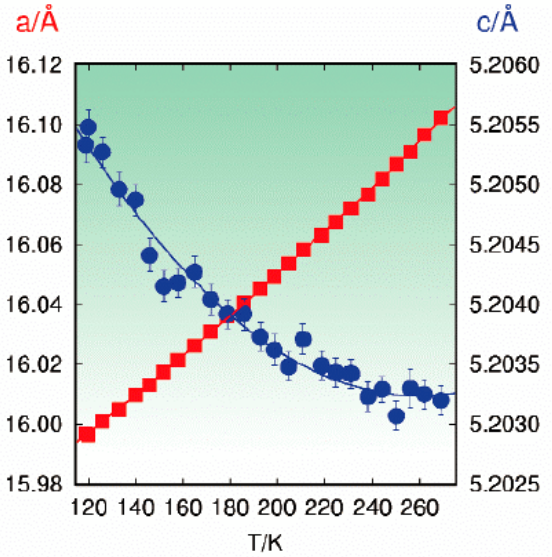

Fig. 4. Thermal expansion of TrpGly·H_2O. It is negative along c.

and/or thermal expansion. In the present case, the total measuring time for 25 temperatures was only 75 minutes.

The evolution of the lattice parameters with temperature is shown in Fig. 4.

The thermal expansion along c, the helical axis, is negative below room temperature and becomes even more negative as the temperature is lowered. At all temperatures, the thermal expansion along a and b is positive and of larger amplitude than that along c, which leads to positive volume thermal expansion. We speculate that this uniaxial negative thermal expansion is caused either by large amplitude motions perpendicular to the helical axis or is due to the water's ordering.

Principal Publication: Angew. Chem. Inter. **41** (2002) 754-755

Structure of Sterol Carrier Protein 2 at 1.8 Å Resolution Reveals a HydrophobicTunnel Suitable for Lipid Binding

(Thomas Choinowski, Helmut Hauser, and Klaus Piontek [ETHZ])

Sterol carrier protein 2, also known as nonspecific lipid transfer protein is an ubiquitous, small, basic protein of 13 kDa found in animals. Its primary structure is highly conserved between different species, and it has been implicated in the intracellular transport of lipids and in a wide range of other *in vitro* functions related to sterol and fatty acid metabolism. Sterol carrier protein 2 deficiency in mice leads to elevated concentrations of phytanic acid in the serum and causes hepato-carcinogenesis

However, its actual physiological role is still unknown. Although sterol carrier protein 2 has been studied extensively in the past 20 years, very little is known concerning its three-dimensional structure. The crystal structure of rabbit sterol carrier protein 2, determined at 1.8 Å resolution with the MIRAS method, shows a unique α/β-fold.

.

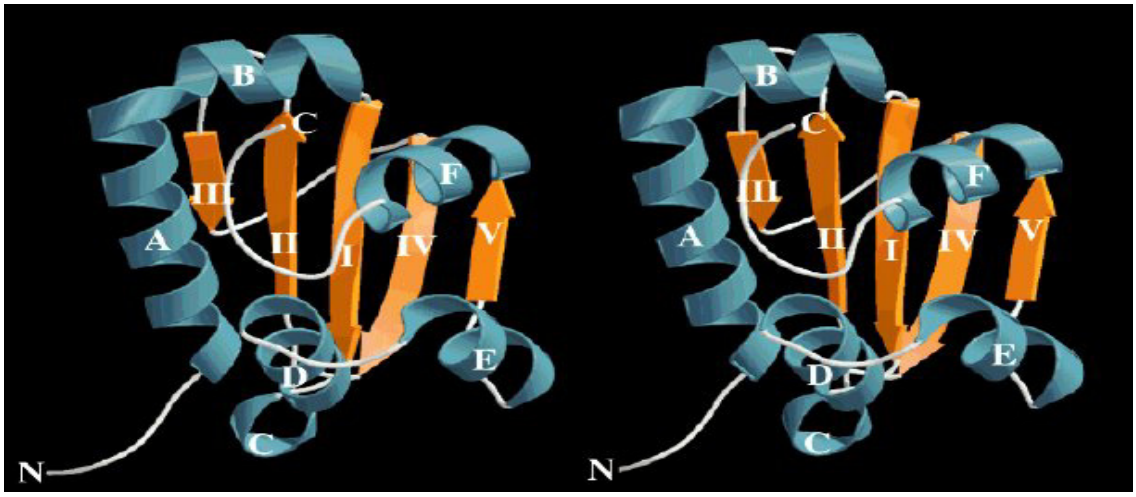

Fig. 5. Stereoview of a ribbon diagram of SCP2 produced showing helices in blue and β-strands in orange.

The core of this protein forms a five-stranded anti-parallel β-sheet flanked by five helices. A C-terminal segment (residues 114-123), together with part of the β-sheet and four α-helices, form a hydrophobic tunnel, providing the environment for apolar ligands such as fatty acids and fatty acyl-coenzyme As. Structurally well-characterized nonspecific lipid transfer proteins from plants have hydrophobic tunnel-like cavities, which were identified as the binding site for fatty acids and related apolar ligands. Despite the fact that plant nonspecific lipid transfer proteins are

- smaller proteins than sterol carrier protein 2,
- show no sequence homology to sterol carrier protein 2, and
- are structurally unrelated,

the cavities of these two classes of proteins are very similar with respect to

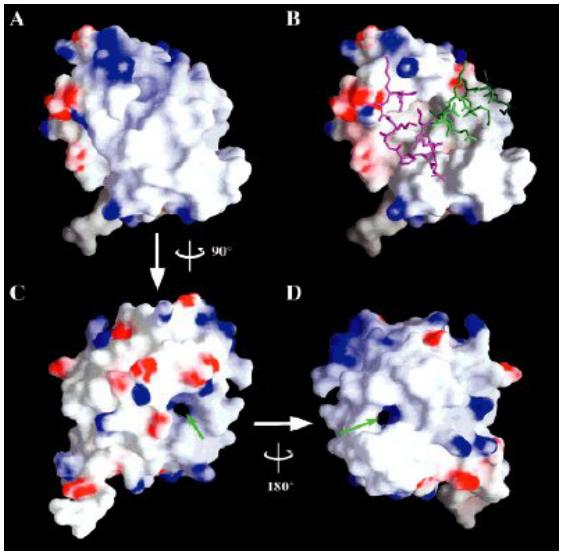

Fig. 6. Electrostatic surface poten-tial of SCP2. Negative surface potentials in red, positive surface potentials in blue, and neutral surface potentials in white. (A) The orientation of SCP2 is as in Figure 5. This side of the molecule is referred to as the front-side. (B) The orientation of SCP2 is the same as in (A), however, R-helix F (green) and the remaining C-terminal portion (magenta) are depicted as stick models. This representation was chosen to delineate the underlying topology of the hydrophobic surface of the tunnel interior. The orientation of SCP2 in (C) and (D) were obtained by a 90° anticlockwise rotation and a 90° clockwise rotation, respectively,of the molecule in (A) about a vertical axis in the plane of the paper. These representations reveal the proposed exit and entrance.

size, shape, and hydrophobicity, suggesting a common functional role.

Principal Publication: Biochemistry. (2000) **39,** 1897-1902

Experimental and Theoretical Identification of New High-Pressure TiO_2 Polymorph

(N. A. Dubrovinskaia, L. S. Dubrovinsky [Bayerisches GeoInstitut, Bayreuth], V. Dmitriev [SNBL], R. Ahuja, V. B. Prokopenko [Geo-sciences, Uppsala], H.-P. Weber [SNBL], J. M. Osorio-Guillen, B. Johansson [Uppsala])

Outstanding properties of some of the titania (TiO_2) polymorphs have not only made those phases extremely useful in sundry applications, but also identified them as prime materials for experimental and theoretical studies.

TiO_2 is of particular interest because of its use in a wide variety of commercial applications including pigment, catalysis, electronics, electrochemical, and ceramic industries and also because of the multiplicity of polymorphs it forms under varying chemical, temperature, and pressure conditions. High-pressure transformations of TiO_2 have attracted special attention because this material is regarded as a low-pressure analogue of SiO_2, the most abundant component of the Earth's mantle. It is well known that titanium dioxide at high pressure attains phases that are isostructural with columbite (orthorhombic α-PbO_2) and baddeleyite (monoclinic ZrO_2).

High-pressure, high-temperature treatment of titanium dioxide yields the α-PbO_2 modification (called also TiO_2II), which can be quenched to ambient conditions.

Combined theoretical and experimental investigations have now led to the discov-

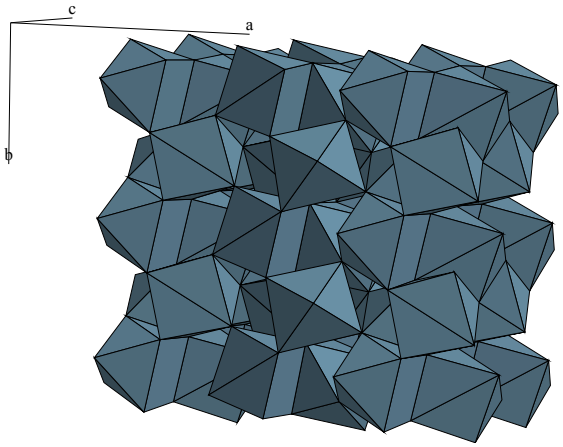

Fig. 7. Polyhedral model for the orthorhombic (space group *Pbca*) TiO_2 phase.

ery of a new polymorph of titanium dioxide, where titanium is seven-coordinated to oxygen in the orthorhombic OI (*Pbca*) structure. The zero-pressure bulk modulus of the new phase measured in the pressure range 19 to 36 GPa is 318(3) GPa. In good agreement with experimental observations and the results of previous theoretical calculations, it is demonstrated that the group IVa dioxides (TiO_2, ZrO_2, HfO_2) on compression at ambient temperature all follow the common path: Rutile **–>** α-PbO_2-type **->** baddeleyite-type (MI) **->** orthorhombic OI (*Pbca*) structure **->** cotunnite-type (OII). In other words, the new orthorhombic structure found is an intermediate phase between the MI and OII structures for the IVa dioxides. In this context one should note that the group IVb dioxides follow another path, and in particular, instead of the baddeleyite-type structure, they transform into the modified fluorite structured cubic phase.

Principal Publication: Phys. Rev. Letters (2001) 87, 275501-275505

An X-ray Absorption Spectroscopic Study on the Local Environment of Copper in CuAlPO-5

(D. G. Nicholson and M.H. Nilsen [Trondheim])

Zeotypic structures (zeolites and aluminophosphates) can incorporate metal atoms in several ways: (1) metal atoms can bind to the internal surfaces that define the channels as well as to the external surfaces. (2) certain metals can substitute for a small fraction of the central atoms within the framework (i.e. aluminium and also phosphorus in the case of the AlPOs). (3) attachment by ion exchange is a characteristic feature of the zeolites because of their charged lattices. Framework substitution of AlPOs occurs for a number of metals such as Li, Be, B, Mg, Si, Ti, V, Cr, Mn, Fe, Co, Ni, Zn, Ga, Ge, As, Zr and Sn. An apparent exception is copper, for which the literature reports several unsuccessful attempts to incorporate copper into AlPO-frameworks. Moen et al. explained this for syntheses involving the secondary and tertiary amine templates, dipropylamine (DPA) and triethylamine (TEA). They found that copper(II) is reduced to copper(I) by these templates at temperatures above 190 ^{0}C. Under these conditions, and in the absence of coordinating anions (e.g. Cl_2), copper(I) disproportionates to metallic copper and copper(II), thereby preventing uptake of copper(II) into the framework. In addition, although these amines do not reduce copper(II) below 190 ^{0}C they still prevent the incorporation of copper into the lattice by forming stable complexes with copper(II). Clearly, molecules possessing templating properties, but which do not complex copper(II), are of interest in syntheses aimed at incor-

porating copper(II) into AlPO's.

Obvious candidates are quaternary amines because they are not Lewis bases yet at the same time can behave as templates.

A copper-containing AlPO4-5 was synthesized using copper(II) oxide as the copper source and tetraethylammonium hydroxide as the template. The local environment about copper in the as-synthesised, calcined and hydrogen-reduced materials has been studied using XANES and EXAFS.

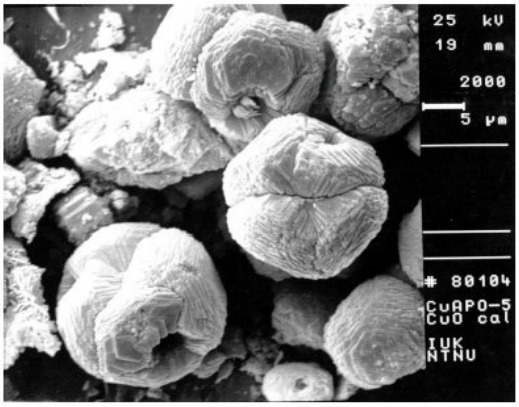

Fig. 8. Scanning electron micrograph of calcined CuAlPO-5.

Results for the as synthesized products:

A. The decreases in the Al **:** P ratio of CuAPO-5 indicate that copper is incorporated into the framework of the zeotype and it would appear that this substitution occurs at phosphorus sites. Structural support for framework substitution is given by the EXAFS of the as-synthesised and calcined materials and by the ESR study by Munoz et al. Interpretation of these structural parameters is consistent with the colours of the products. In the turquoise as-synthesised materials the copper environments are tetragonally distorted octahedra in which the axial positions are possibly occupied by hydroxy groups. In the grey calcined material (550C) coordination to the framework is increased by a further two bonds to framework oxygen atoms and the symmetry degrades from a tetragonally distorted octahedron to a non-tetragonally distorted octahedron for which the coordination is increased from distorted tetrahedral by two longer bonds to framework oxygens. On further calcinations (800C) the microporous structure breaks down and copper is free to reassert its preference for the tetragonal octrahedral environment and a turquoise colour.

B. The XANES spectra of the Cu-β zeolite and CuAPO-5 show that the latter differs from the copper ion-exchanged zeolite in not undergoing autoreduction.

C. XANES and EXAFS show that copper(II) in CuAPO-5 is reduced to large particles (w40 A) upon reduction in hydrogen.

D. CuAPO-5 is a relatively poor catalyst for reducing NO in the presence of NH_3 and O_2 (Fig. 9). However, putative CuAPO-5 synthesised from copper(II) acetate is a significantly better catalyst

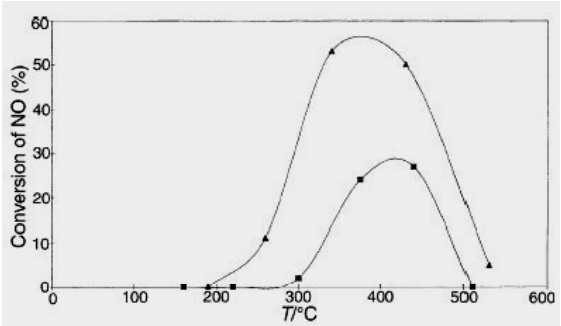

Fig. 9. Catalytic activity of CuAlPO-5 for the selective catalytic reduction of Nox in the presence of NH_3 and O_2. Square: Sample A; copper(II) as Cu source. Triangle: Sample B: copper (II) acetate as copper source.

Principal Publication: J. Mater. Chem.. (2000) **10**, 2562-2566

CATALYSIS

Within the SNBL there are several groups, both in CH and in N, actively working in this field. Some are interested in the details of the catalytic processes, others in devising new materials as supports for catalysts.

X-Ray absorption spectroscopy (XAS) – one of the four techniques available at SNBL- is a widely used method for characterizing local structural features of selected elements in heterogeneous catalysts. In particular, although the technique is actually a bulk technique it is also valuable for studying chemical reactions that take place at the surfaces of heterogeneous catalysts because the overall contribution to the XAS signal arises from the significant proportion of active sites that are highly dispersed over a large number of surfaces. XAS has been used extensively to study local metal environments in a number of zeotypes. Examples include metal-substituted microporous alumino- and silicoalumino-phosphates (AlPOs and SAPOs) and the cations in ion-exchanged zeolites.

Fe/ZSM-5 Prepared by Sublimation of $FeCl_3$: The Structure of the Fe Species as Determined by IR, ^{27}Al MAS NMR, and EXAFS spectroscopy

(P. Marturano, L. Drozdova, A. Kogelbauer and R. Prins [ETHZ])

Owing to their redox properties, iron-exchanged zeolites have been investigated for many years. Recently these catalysts have attracted renewed attention as it has been shown that Fe/ZSM-5 with a high degree of ion exchange (Fe/Al ~ 1) possesses remarkable properties for the selective catalytic reduction of nitrogen oxides (NOx) by hydrocarbons. Besides its having a higher activity than Cu/ZSM-5, especially its insensitivity towards the presence of H2O and S02 as well as its exceptional hydrothermal stability make Fe/ZSM-5 stand out among the zeolite-based catalyst systems.

The state of the iron in two different Fe/ZSM-5 samples prepared by sublimation of $FeCl_3$ was investigated by EXAFS, IR, ^{27}Al MAS NMR, XRD, and nitrogen adsorption measurements. In one Fe/ZSM-5 (Fe/Al =1) sample, EXAFS revealed for the first time the presence of diferric (hydr)oxo-bridged binuclear clusters, whose structures differ from those postulated in the literature, resembling that of the methane mono-oxygenase enzyme. IR showed that binuclear Fe complexes are located at the ion-exchange positions of the zeolite, compensating one or two lattice charges. The remainder of the charge-compensating sites are Bronsted hydroxyls. On both zeolites, the NMR detection of the framework Al atoms (54 ppm) is strongly perturbed by the paramagnetic effects induced by the Fe ions. The intensity of this peak parallels that of the Bronsted hydroxyls in the III spectra, thus reflecting the presence of Fe species at ion-exchange positions. In a second Fe/ZSM-5 (Fe/Al = 0.8) sample, the iron was present predominantly in the form of large hematite particles (EXAFS, XRD), although a minor fraction of binuclear species might be present as well. The formation of different species seems to be related to different hydrolysis processes occurring on the two zeolites upon washing of the preparation after the sublimation of $FeCl_3$. It is also suggested that the final state of the Fe depends on the presence of extra-framework Al species as well as the crystallite size of the zeolite used.

NOVEL AND UNUSUAL MATERIALS

Advances in device technology is being driven, amongst other factors, by development of new materials. With increasing frequency, these materials will have been designed with the help of modeling programs, and their properties predicted. Such was the case in the recent development of a new battery material. However, theoretical predictions need experimental confirmation. As samples can often be synthesized only in minute quantities, access to synchrotron radiation is therefore often of crucial importance in ascertaining the correctness of the predicted crystal structure.

Ti_3Al: Its Structural Behaviour under Pressure up to 25 GPa

(N.A. Dubrovinskaia, M. Vennstroem, I.A. Abrikosov, R. Ahuja, P. Ravindram, Y. Andersson, O. Eriksson, V. Dmitriev and L.S. Dubrovinsky [Uppsala and SNBL])

Titanium and its alloys are traditional engineering materials that possess an extraordinary combination of properties. They are commonly utilized in aerospace and in the petrochemical industries. In particular, the phase Ti_3Al (Ni_3Sn structure type) exhibits low density and good high-temperature strength and was therefore chosen for the development of aircraft engines materials.

However, one of the main technological problems with Ti_3Al is its brittleness. In practice, the ductility can be increased by alloying Ti_3Al with 8–18 % Nb (other possible alloying elements are Mo, V, Ta, and Ni), but other more efficient ways to increase the ductility are being pursued. One promising avenue is to increase the number of active slip planes to satisfy the von Mises criterion. Crystal structure plays a very important role in influencing the ductility. For this reason, the goal is to transform the material of interest, which has tetragonal symmetry, into one with cubic symmetry, since cubic structures often display many more active slip planes. It is for this reason that a structural investigation of Ti_3Al as a function of p and T has become relevant. If one gets a good grasp of the factors influencing its structural stability, one may then find ways to synthesize this material in a cubic (and hopefully more ductile) form.

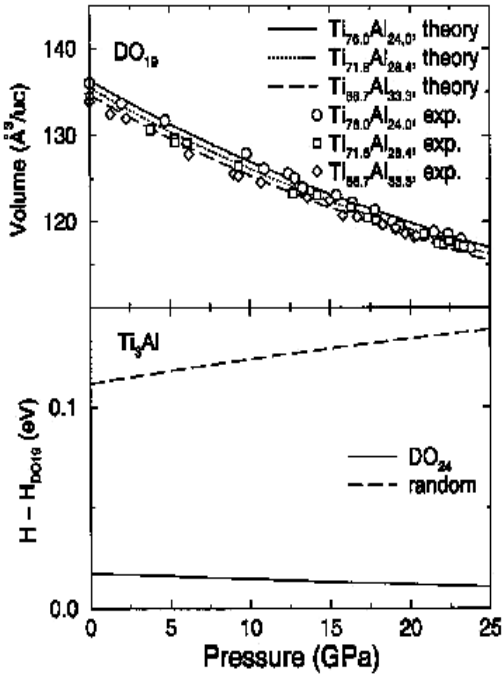

Fig. 10. Dependence between unit cell volume and pressure.

(top) *Experimental (circles, squares, and diamonds) and theoretical lines for the Ti_3Al alloys with 24 at. % Al (solid line, circles), 28.4 at. % Al (dotted line, squares), and 33.3 at. % Al (dashed line, diamonds). Theoretical results are obtained by the LMTO-ASA-CPA method. The FP-LMTO PV diagram for ordered Ti_3Al is not shown, but is in very good agreement with those for off-*

stoichiometric alloys presented in this figure

(bottom) *Calculated pressure dependence of the enthalpy H for stoichiometric Ti_3Al with DO 24 structure (solid line, FP-LMTO calculations) and disordered hcp Ti_3Al alloy (dashed line, LMTO-ASA-CPA calculations) relative to the enthalpy of ordered DO Ti Al.*

Experimental high-pressure studies of titanium aluminide (Ti_3Al) have been carried out under quasi-hydrostatic and non-hydrostatic conditions up to a pressure of 25 GPa using an *in situ* powder x-ray diffraction technique

The experimental equation of state for three samples with different compositions was fitted using the Birch-Murnaghan equation. The parameters obtained agree very well with theoretical results (see Fig. 10). In the pressure range studied neither experiment nor theory revealed any pressure-induced structural phase transition. In particular, the phase transition from the DO_{19} (Ni_3Sn type) structure of Ti_3Al to DO_{24} (Ni_3Ti type) structure, reported earlier by Sahu *et al.* (Phys. Rev. Lett. 78, 1054 (1997)) was not confirmed.

Powder Diffraction and Inelastic Neutron Scattering Studies of the Na_2RbC_{60} Fulleride

(K. Prassides, C. M. Brown, S. Margadonna, K. Kordatos, K. Tanigaki, E. Suard, A. J. Dianoux and K. D. Knudsen
[Sussex, ILL, Osaka and SNBL])

Even though no superconductivity has been encountered for alkali fulleride compositions other than $A_2A'C_{60}$ (A, A'=Na, K, Rb, Cs), a genus of the fulleride family with composition AC_{60} (A~K, Rb, Cs) has also attracted considerable interest, principally because of the variety of structural forms encountered. Besides the formation of metastable cubic and dimer structures formed by quenching to low temperatures, direct C-C bonding between the C_{60} ions leads to polymer chain formation. The resulting materials adopt quasi-one-dimensional orthorhombic or monoclinic structures (space group Pmnn and I2/m), with the shortest center-to-center interfullerene distance of the order of 9.10 Å, consistent with the formation of two C-C bridging bonds. For a while, it seemed that formation of bridged fulleride ions was confined to C_{60}^{-} and $C_{59}N^{12}$ units which contain a single unpaired electron in the lowest unoccupied molecular orbital (LUMO). However, recent work on sodium fullerides has led to the realisation that such systems are much more abundant than hitherto appreciated, as polymeric systems containing the C_{60}^{3-} and C_{60}^{4-} ions were synthesized and structurally characterised. For instance, Na_2RbC_{60}, whose ground state structure was thought for a long time to be primitive cubic, was found to form, upon slow cooling, a metallic monoclinic polymeric structure (space group P21/a, a~13.71, b~14.55, c~9.37 Å and β~133.53 deg) distinctly different from that of the AC_{60} salts, with the short interfullerene distance along c implying the formation of a single C-C bridging bond. Such a structure has also been found to form for other sodium and lithium salts, including the $Na_2Rb_{1-x}Cs_xC_{60}$ quaternaries at ambient and elevated pressure and Na_2CsC_{60} and Li_3CsC_{60} at elevated pressure. On the other hand, Na_4C_{60} gives rise to a two-dimensional polymer in which the interfulleride bonding is of single C-C bond order between four C_{60}^{4-} nearest neighbours.

The present study is a comprehensive one. It determines the structural and vibrational properties of the Na_2RbC_{60} salt using a combination of experimental techniques.

Powder synchrotron X-ray and neutron diffraction were employed to study in detail the monomer to polymer transformation, both as a function of temperature and time. Neutron inelastic scattering measurements were used to characterise both the intramolecular vibrational spectrum of C60 32 and to provide direct spectroscopic identiÆcation of the interfullerene C±C bridging modes in the intermolecular energy region. Neutron and synchrotron

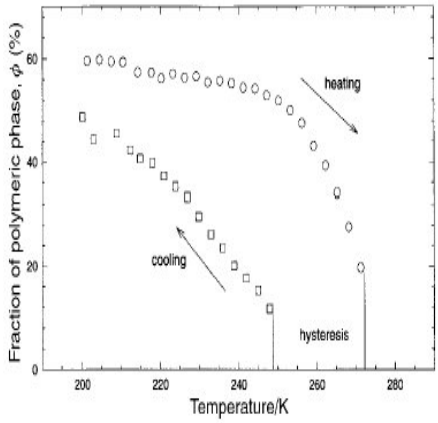

Fig. 11. Temperature Evolution of the Volume Fraction of the mcl phase of Na_2RbC_{60} as obtained from Rietveld analysis of synchrotron X-ray powder diffraction data during cooling and heating cycles.

X-ray powder diffraction and inelastic neutron scattering (INS) studies of Na_2RbC_{60} in both its polymeric and monomeric phases have been performed as a function of temperature, with particular attention paid to the cooling protocol.

The powder diffraction measurements on cooling confirm the slow transformation of the primitive cubic high temperature phase to the monoclinic low temperature phase in the vicinity of 250 K. Rietveld refinements of both the X-ray and neutron data show that over half of the sample transforms to the polymer in the temperature range 180±200 K, this fraction rising to 64(2)% at base temperature (Fig. 11). On heating, the percentage of the monomer phase increased from 230 K at the expense of the polymer, with a full transformation occurring by 277 K. A final phase transition to the disordered fcc structure occurs over a range of temperatures from 299 to 317 K. Study of the time evolution of the monomer A polymer transformation at 180 and 200 K allowed us to extract an estimate of the activation barrier to interball C-C bond formation as 0.16 (2) eV, comparable to the magnitude of the reorientational potential in the precursor monomer phase. INS spectra in the temperature range 100 to 320 K confirm the reduction of symmetry from the primitive cubic phase through splittings of the intramolecular vibrational modes. The polymeric nature of interfullerene bonding in Na_2RbC_{60} is also confirmed via direct observation of excess scattered intensity in the 8 ± 25 meV region of the generalised phonon density-of-states (GDOS).

Electrical-field-induced structural changes in deuterated potassium di-hydrogen phosphate

(S.J. van Reeuwijk, A. Puig-Molina and H. Graafsma [ESRF])

The electric-field induced distortions in the unit cell of both KDP (KH_2PO_4) and DKDP (KD_2PO_4) were measured as a function of temperature using x-ray diffraction. For both compounds the d_{36} shows a Curie-Weiss behavior, with constants 3.61(3) x 10^{-9} KC/N for KDP and 4.4(2) x 10^{-9} KC/N for DKDP. For DKDP the electric-field induced change in integrated intensity of a number of reflections were measured at room temperature, using the KUMA6-CH high-resolution single-crystal diffractometer at the SNBL. These changes were submitted to a refinement where the shifts of the atoms and the ordering of the deuteriums were determined.

In the presence of an electric field of 2.7×10^6 V/m parallel to the *c* axis, the P atom is displaced by $27(3)10^{-4}$ Å along the *c* axis, and a redistribution of the deuteron over the two formerly equivalent sites takes place. The site towards which the P atom moves is decreased in occupancy in favor of the other by an amount of 0.8(2)%. The distortion of the oxygen framework is marginal. These results agree very well with experiments where the phase transition was induced by cooling below T_C. On the basis of the structural changes, the calculated electric-field induced polarization was 0.18(4) $\mu C/cm^2$, consistent with other experiments. Based on our findings we discuss the sequence of the main structural changes involved in the phase transition.

Low-Temperature Form (Phase II) of Ionic Conductor Ag_7TaS_6 Analyzed using High-Resolution Synchrotron X-ray Powder Diffraction Data

(M. Onoda, H. Wada [Tsukuba], P. Pattison [SNBL], A. Yamamoto, M. Ishii, G. Chapuis [Lausanne])

The ternary sulfide Ag_7TaS_6 displays high Ag-ion conductivity at ambient temperature. Its cubic structure is apparented to the argyrodite family, with the Ag ions distributed statistically over many sites of different coordination. Below ~280K this phase I transforms to another structure of monoclinic symmetry; at even lower temperatures, below ~170K, this phase II converts to yet another phase, Ag_7TaS_6 III.

Synchrotron radiation powder diffraction data have been measured at 240K on phase II, with the goal of determining the thermal parameters of the Ag ions and contrast them with those of the ambient temperature phase I. Thanks to the narrow width of the reflections, even at high angle, and their increased intensity, relative to ambient temperature, individual thermal parameters for the Ag ions could be determined. From the seven (7!) Ag sites in the structure four exhibit unusually large apparent thermal parameters, which were interpreted as due to disordering of these Ag ions over their conduction paths.

METHODOLOGICAL DEVELOPMENT

Three-beam Interference Measurements with a Six-Circle k Diffractometer

(G. Thorkildsen, H.B. Larsen, R.H. Mathiesen and F. Mo [Stavanger and Trondheim])

The physical estimation of triplet phases is based on the evaluation of so-called Ψ scan profiles; that is, the intensity pattern for a primary reflection (hkl) mapped out during the rotation about its reciprocal-lattice vector, **h**, retained in the scattering position, while a secondary lattice node is passing through the Ewald sphere. Thorough reviews of this technique have been presented by Chang (1992) and, more recently, by Weckert & Hummer (1997). Experimentally, the most efficient way of obtaining such profiles is by using a specially designed six-circle Ψ–diffractometer. This instrument consists of an Eulerian cradle with two extra axes enabling a pure Ψ rotation about a single axis. In 1997, a newly designed six-circle multipurpose κ diffractometer was installed at the Swiss-Norwegian beamline (SNBL) at the ESRF. A schematic drawing of the instrument is shown in Fig. 12 (a). We here report on the application of this instrument for three-beam diffraction.

A procedure for calculating the correct angle setting for a specific three-beam situation on a six-circle κ -diffractometer was outlined. It was experimentally shown that interference profiles can be recorded using this approach. It was shown that three-beam intensity profiles may be obtained with a six-circle κ diffractometer using ω for the Ψ rotations, but the potential for making such measurements, with a subsequent reliable estimation of triplet phases, is restricted (Fig. 12 (b)).

The open construction of the κ goniostat allows, however, greater freedom in real space, e.g. for mounting various sample stages, such as pressure cells, cryostats, furnaces, etc., but access to reciprocal space is limited compared, for instance, with Eulerian cradle instruments.

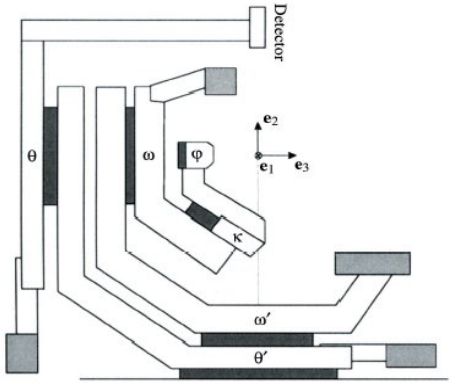

(a)

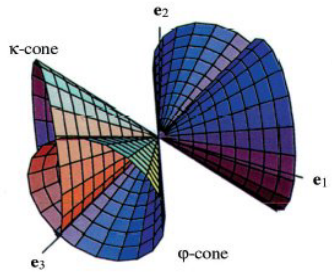

(b)

Fig. 12. (a) The KUMA6-CH six-circle diffractometer (b) Access restriction to reflections offering full Ψ scans –due to Kappa geometry.

Improvement in flux density on both beamlines

(Herrmann Emerich, Wouter van Beek, Marc Pissard, all SNBL)

The increase in flux density was needed to be able to investigate smaller protein crystals, as smaller specimens are easier to grow and do not break up in a cryogenic measurement environment. A typical protein crystal has a size of 50 µm in the largest dimension. Up till now, the existing optics on SNBL's beamlines produced a focal spot of 500 µm. A narrower beam with a higher flux density but a smaller total integrated flux would obviously be better matched to today's crystal sizes.

Smaller sample volumes are encountered not only in protein crystallography, but also in experiments at non-ambient conditions (low and high temperature; high pressure), where the experimental technique imposes the use of unusually minute specimens.

An extensive survey of the different types of existing focussing devices was carried out, with the aim to either acquire or develop in-house a suitable system. A large variety of solutions were envisaged, all with their own specific advantages and drawbacks. Finally, we opted for a condensing capillary, for a variety of reasons, which include:

- its ability to produce a 50 µm spot
- its ease of alignment (little disruption of the busy user schedule)
- its moderate cost
- and the fact that such beam condensors had been shown to perform well at other synchrotrons, for the exact same purpose.

Such a capillary was designed in collaboration with and purchased from one of the world leaders in this field, D.H. Bilderback, from CHESS (Cornell University, USA). In order to insert and test this new device, ancillary equipment had to be purchased and commissioned. The new equipment consists of alignment stages, additional stepper motor channels, an x-ray camera to inspect the focus, and a new control system to handle the additional channels. These investments in ancillary equipment paid off, not only in the proper handling of the capillary but also in streamlining the daily operation of the beamlines. (e.g. easier wavelength changes, quicker aligning of sample stages).

The capillary has now been tested, and the results matched our expectations: a gain by a factor of four in flux density on a spot as large as 50 µm was easily reached (see fig. 13).

The ideal shape for a focussing capillary is obviously elliptical. However, such a capillary is very difficult to produce. This prompted us to try an idea for a 'new' and improved focussing device. Our prototype consisted of two vertically placed pieces of commercial float glass to which we gave a cylindrical shape. This very crude set-up already outperformed the commercial capillary by a factor of 2 to 3 x; this encouraged us to pursue this path, with a more sophisticated design. At present, we are working on a mirror of such a shape that upon bending it becomes elliptical. Another advantage of this device wrt the capillary is that the focal point can be located far away (~15 cm or more) from the beam condenser. By 2001/2002 we ought to have a device ready for user operation. In parallel, we will continue to develop the concept further as there is much room for improvements (coatings, Kirkpatrick-Baez arrangement).

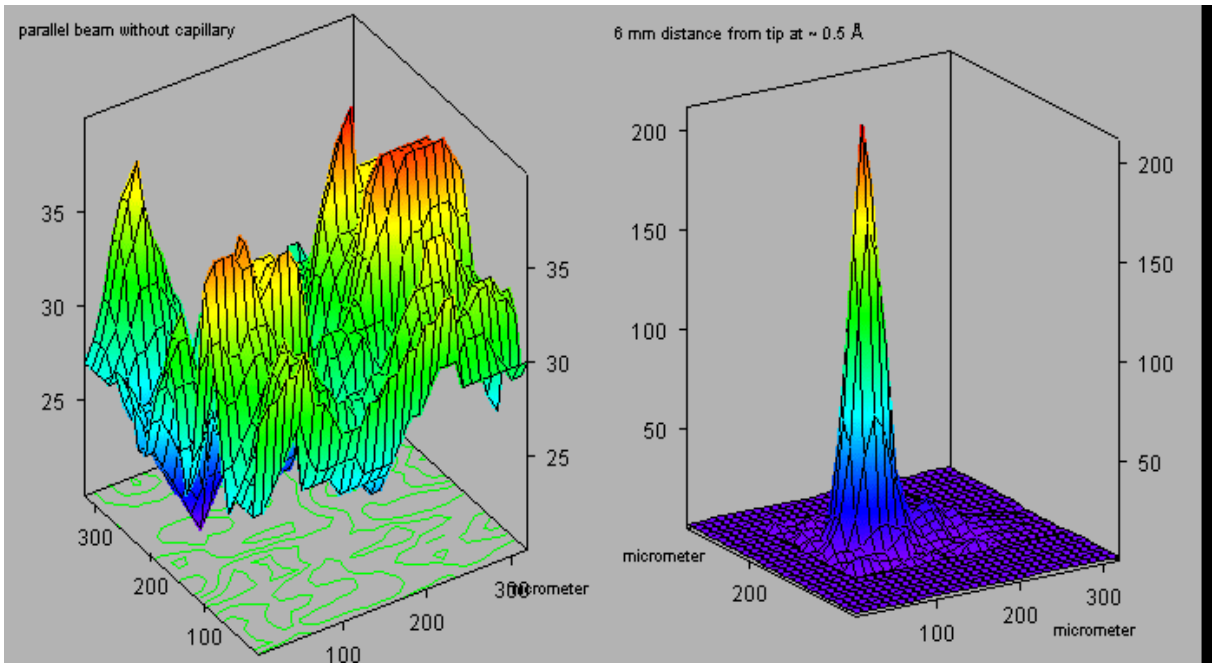

Fig. 13. Effect of focussing capillary on beam.
(Left: Without focussing capillary. Right: With focussing capillary)

Development of a Wire Detector for the Swiss Light Source

(Stéphane Burger [SLS, now CERN], Phil Pattison [SNBL]), Rafael Abela [SLS])

A beam profile / position monitor has been designed and tested at the SNBL. The primary aim of this development: To check whether the beam is well centered with respect to the primary slits. The secondary aim: To measure the beam structure as well. The SNBL is built on a bending magnet source. Such a source emits a fan of radiation, the intensity of which is uniform in the horizontal and Gaussian in the vertical direction. Particular attention was focussed on the vertical profile of the beam. To this purpose, a filter rack including a manipulator was used as a basis for the new BPM.

The principle of this wire detector consists in measuring the current generated by the photon beam in a tungsten wire passing through the beam. The current generated by the photoemission effect is proportional to the intensity of the beam.

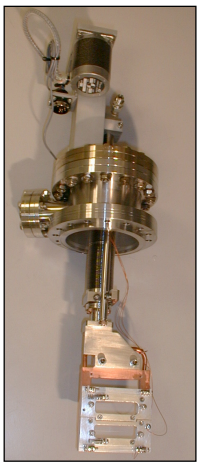

This monitor has been installed behind the splitter vessel, right after the front end. It then scans the part of the beam going to station A, 25 meters from the source (2mrad at 25 meters → 46mm) The power density at this point is 0.95W/mm^2.

Fig. 14: Picture of the complete monitor.

A tungsten wire is being used because of its good mechanical and electrical characteristics:

- thermal expansion 4.3×10^{-6} [K^{-1}]

- thermal conductivity 177 [W/m.K]

Concerning the heat, the calculation gives us a margin of security because the maximum temperature the wire can reach is 2400K at 200mA that is to say 1300K below the melting point of the tungsten which is about 3700K. Thus, a cooling system is not really needed. At the temperature of 2400K, the thermal expansion gives a lengthening of 0.75mm for a 80mm length. It is the worst case we can have.

The first test was made with monochromatic beam, is shown in Fig. 15,

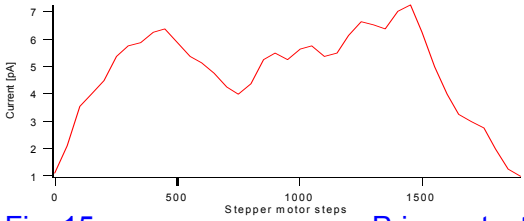

Fig. 15: Primary test in monochromatic beam, in air, without any shielding.

and was rather encouraging as it showed both the profile of the monochromatic beam as well as the position of the capillary used as a reference in the center of the beam.
After the installation on the beamline, in vacuum, we started the tests.

Reproducibility

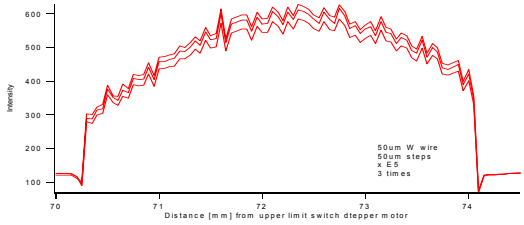

Fig. 16. Reproducibility of 50 μm wire, with several identical scans.

Effect of the scanning step size on the profile

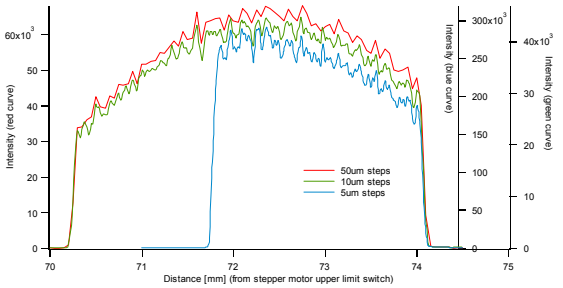

Fig. 17: Different scans with the 50 μm W wire made with 50, 10 and 5μm scanning steps.

Effect of the size of the wire on the resulting profile

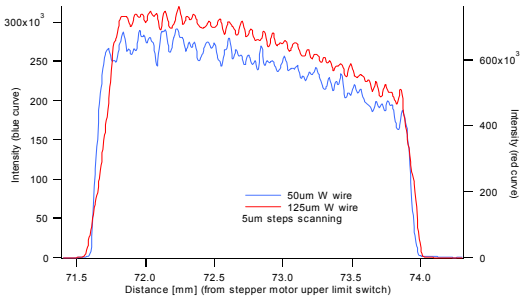

Fig. 18. Comparison of scans done with the 125 μm wire and the 50 μm wire (5 μm steps).

Resolution and function of the size of the W wire diameter

In the ideal case, the width of the edges of the profile should be the diameter of the wire. That is what we check in the two following figures 19 and 20.

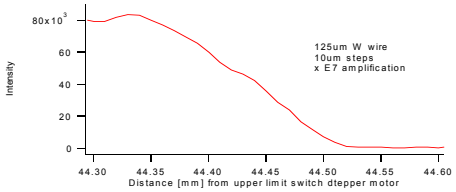

Fig. 19: One of the edges of the profile given by a scan using the 125μm diameter W wire.

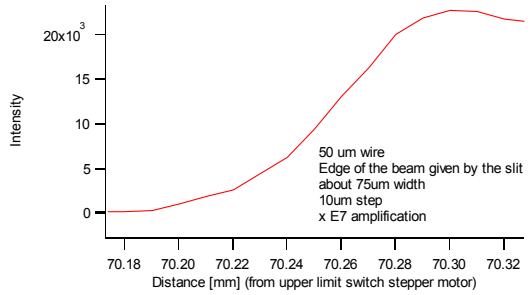

Fig. 20: One of the edges of the profile given by a scan using the 50μm diameter W wire.

Summary

Whatever the diameter of the wire, the reproducibility of the results with this device is very good, even with a different amplification

The current given on the wire at any position is always the sum of the signal generated over the thickness of the wire. Then, it is obvious to say that thinner the wire, better the resolution. The scanning step size and the diameter of the wire are then two factors that play a role on the profile result as it is shown

Optimizing the positioning of the slits revealed that the actual beam was not ideally centered. With the help of this monitor it was then easy and fast to “peak up” the beam. The reason why the beam was initially not optimally defined was to protect the first mirror.

We had the opportunity to check the monitor off-line during one of the shutdowns. No visible damage could have been seen on the wires.

In summary, this device perfectly fulfills our expectations and resulted an improvement of the beamlines’ performance. Its simple design and ease of use make this monitor a very useful device for profile capture, quick alignment, detecting problems and also as a BPM.

Prototype of a Photon Beam Position Monitor in test on SNBL at ESRF

(Chen Qianhong, Juraj Krempasky, and Stéphane Burger [SLS / SNBL])

A prototype of a beam position monitor has been designed and manufactured at the Paul-Scherrer Institute. It is based on the Bessy staggered-pair-of-blades principle (SPM).
A pair of blades is positioned in such a manner that it protrudes vertically into the edges of the beam, as shown in Fig 21. If the beam is perfectly centered in the middle of the 2 blades. the photoemission effect will generate an equal current from each blade. On the other hand, a drift of the beam would increase the current on one of the blade and decrease the other. Basically, the beam position is deduced from these currents after amplification and processing of the data with the equation:

$$Pos = C.\frac{A-B}{A+B}$$

The device was installed on the Swiss-Norwegian beamline (SNBL) at ESRF during the May 2000 in order to test it wrt reproducibility, effect of bias voltage, effect of beam refill, etc and to determine its general characteristics.

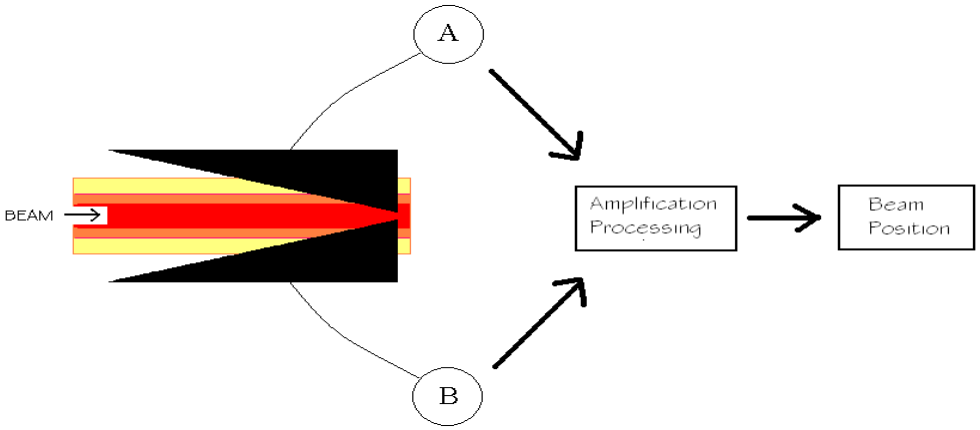

Fig. 21. Principle of the beam position monitor.

The monitor was shown to be very reliable as it yielded about the same values as the ESRF XBPM. The biasing option turned out to play an important role in the performance of the monitor as it improves the S / N ratio and extends its linearity range. Resolution is of the order of a micrometer (it is difficult to check this characteristic more precisely since the beam is continuously moving by a few μms); its performance is linear over 1mm (see Fig. 22) and its reproducibility is excellent. At least one unit each of this now tested design is to be installed on each bending magnet and wiggler front-end at the SLS.

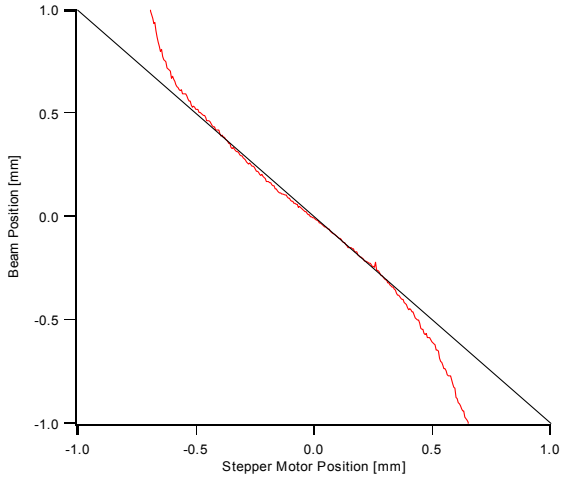

Fig. 22. Linearity of the beam position monitor.

SINGLE CRYSTAL DIFFRACTION – KUMA SIX-CIRCLE DIFFRACTOMETER. The KUMA is fully operational, but we are still using the original control software on a DOS platform. A development version of the new software was tested during the October shutdown. The instrument has been used for experiments in high-pressure crystallography using diamond anvil cells, measurements of satellite reflections in incommensurate crystals, the study of shifts of diffraction peaks under the influence of applied electric fields and accurate charge density measurements. A new detector has been purchased with an improved dynamic range (up to 10^6 cps).

Funds are now available for a cryostat, and we are currently evaluating different commercial products. It should be feasible to install the same device on the MAR345, and this opens up some interesting possibilities in low-temperature crystallography.

SINGLE CRYSTAL DIFFRACTION – MAR AREA DETECTOR. A major new development for the MAR has been the successful use of diamond anvil cells for high-pressure dta collection. The combination of a DAC and the focused SR beam on BM1A provides sufficient flux for measurements around 500 kbar. Several groups (ETHZ, Lausanne and SNBL) have already collected data in this mode. A group from the University of Bern has measured the temperature dependence of diffuse scattering using the area detector. Temperature-dependent phase transitions have also been studied with the MAR, as well as accurate measurements of the lattice constants as a function of temperature (+- 0.0001 Å).

In another development, a scanning slit system has been designed and constructed for use with the MAR. By exposing different parts of the MAR at different times, the intrinsic time resolution of a powder pattern can be reduced to a few seconds.

HIGH RESOLUTION POWDER DIFFRACTION

The diffractometer has now been upgraded to operate with 4 (eventually 6) analyzer crystals, and the software for binning the data has been fully implemented. The analyzer crystal set-up has been calibrated between about 0.4 and 1.2 Å. The data collection time for a full powder pattern has been reduced from about 24 hours to 8 hours. There is a need for a high-temperature furnace, and an in-house development to build such a device is in progress.

.

EXAFS. The EXAFS spectrometer has been operating with a combination of channel-cut monochromator and mirror for harmonic rejection, and many spectra have been collected in this mode in the spectral range from about 6.5 keV at the Mn K-edge to about 40 keV at the Ce K-edge. A high angular resolution encoder has been installed to ensure that angular accuracy at 40 keV (where the angular movements between steps are very small) is sufficient for high quality EXAFS scans.

PRODUCTIVITY OF THE FACILITY. The use of the beamlines has stabilized over the last 3 years at around 500 shifts (167 days) per beamline per year. This total includes the beamtime allocated to the ESRF for public use. These numbers compare very favorably with other CRG beamlines (see Fig. 23). The average beamtime allocation per project is about 10 – 12 shifts, and each project can, of course, include several samples. With the increased throughput on the powder diffractometer and the MAR area detector, we are now able to produce several hundred data sets per year.

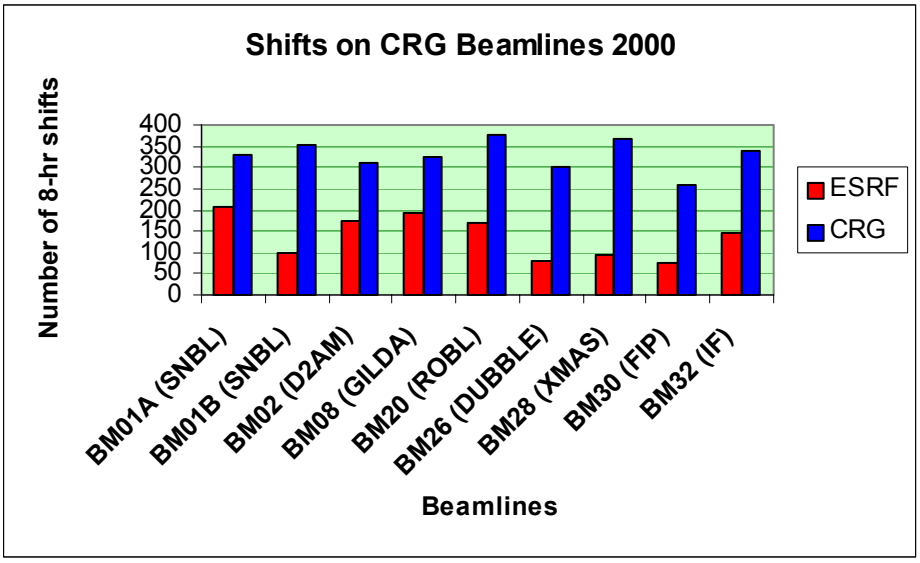

Fig 23. Beamlines' Productivity (Number of shifts delivered to users).

Time allocation (in % of totally available beamtime) to each instrument is shown in fig. 24. Compared to previous years, there has been a marked increase in the use of the EXAFS spectrometer.

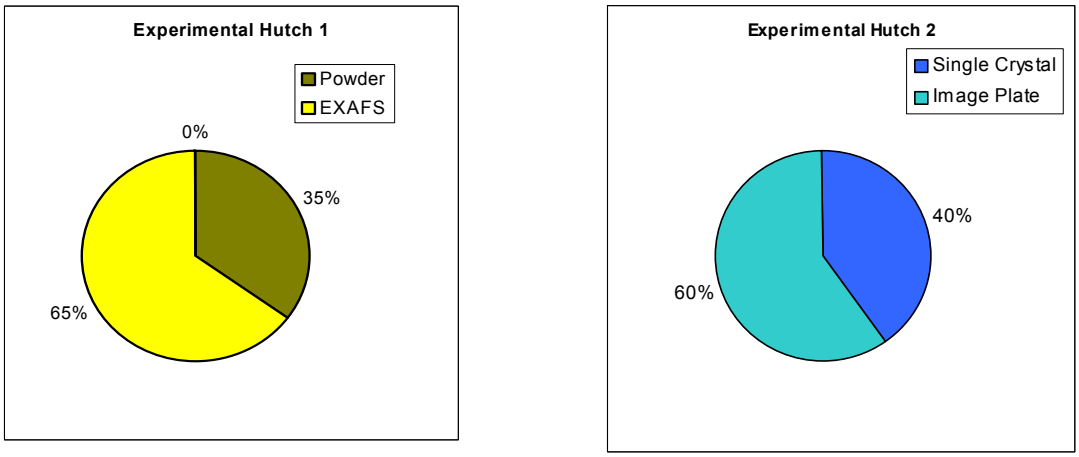

Fig 24. Allocation of Beamtime to Instruments.

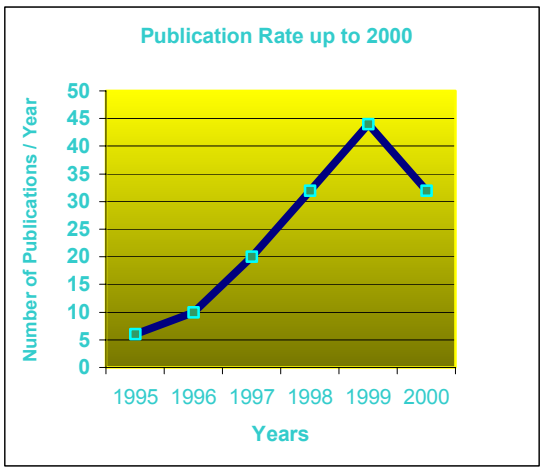

Fig. 25. Annual Publication Rate of Publications Based on SNBL Data.

Another indicator of the beamlines' productivity is the publication rate over the past several years (see fig. 25).

It takes into account all publications using data collected on the beamlines, irrespective of the national origin of the users. Note that there is usually a delay of about 12-18 months between data collection and the publication of results, and this accounts for the scatter.

BEAMLINES PERSONNEL (1999 – 2000)

	Function	Occupation Rate
Hans-Peter Weber	Project Director	0.65 SNBL / 0.35 UNIL
Philip Pattison	Beamline Scientist	0.75 SNBL / 0.25 SLS
Jon-Are Beukes	Norwegian post-doc	1.0
Silvia Chiara Capelli	Norwegian post-doc	1.0
Hermann Emerich	Senior Engineer	1.0
Wouter van Beek	Junior Engineer	1.0
Oleksei Kuznetsov	PhD Student	1.0
Chantal Seferiadis	Executive Assistant	1.0
Marc Pissard	Senior Technician	1.0
Stéphane Burger	SLS Junior Engineer	Visiting

STEERING-AND-OVERVIEW COMMITTEE (1999 – 2000)

David Nicholson (NTNU)	Chairperson
Joerg Kallen (Roche)	Member
Hans-Beat Buergi (Bern)	Member
Ed Hough (Tromso)	Member
Martin Kunz (ETHZ)	Member
Hans-Peter Weber (SNBL)	Member
Philip Pattison	Secretary

-RAY STRUCTURES ROM POWDERS

v method gives single-crystal-like raction data from polycrystalline samples

ıe most powerful way to deter- nine the atomic structure of a rystalline material is to perform diffraction experiments on a sin- /stal (usually at least 50 µm on an . But many important materials olycrystalline—they cannot be as single crystals of large enough and this has stymied efforts to ate their structure.

w, researchers at the Swiss Federal te of Technology in Zurich—better by its German acronym ETH— ound a direct way to determine the ıre of many polycrystal- aterials, in essence by ex- g single-crystal-like dif- n data from these materi- ıe new approach allows etermination of crystal ures "as complex as

tal consists of isolated spots (refle tions) of varying intensities," and the i tensities are used to find the locations the atoms in the crystal. The solution structures from such data has becom almost routine, McCusker notes.

However, when a single crystal cann be grown, researchers must resort t powder diffraction methods, which ar less powerful and often not successfu Normally, a powder diffraction pattern measured on randomly oriented cryst lites, McCusker says. In the best circun stances, "this leads to a superposition

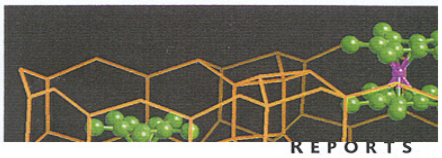

REPORTS

Single-Crystal–Like Diffraction Data from Polycrystalline Materials

Thomas Wessels, Christian Baerlocher, Lynne B. McCusker*

A method for solving structures from powder diffraction data was developed and its validity was demonstrated on three complex structures. The metho uses a textured sample and exploits the high intensity and parallel nature o synchrotron radiation. In principle, crystal structures as complex as those routinely solved by single-crystal methods can be determined with this ap- proach. For example, the as-synthesized form of the zeolite UTD-1, with 6 nonhydrogen atoms in the asymmetric unit, could be solved directly. With thi method, a larger range of structural complexity becomes accessible to scientist interested in the structures of polycrystalline materials that cannot be growr as single crystals.

ny industrially important materials, rang- from ceramics to catalysts to pharmaceu- ıls, are polycrystalline and cannot be wn as single crystals. To understand the perties of these materials, structural infor- tion on an atomic level is essential. How- can be handled falls well below that could be tackled with single-crysta This is not surprising: A one-dime powder diffraction pattern necessaril tains less information than does its dimensional single-crystal counterpart.

A Glycyl Radical Site in Crystal Structure of a Cl Ribonucleotide Reducta

Derek T. Logan,[1]* Jessica Andersson,[2] Britt-Marie Pär Nordlund[1]*

ibonucleotide reductases catalyze the reduction of ribonucleo ibonucleotides. Three classes have been identified, all using fre stry but based on different cofactors. Classes I and II have be volutionarily related, whereas the origin of anaerobic class I lusive. The structure of a class III enzyme suggests a commo hree classes but shows differences in the active site that can n the basis of the radical-initiation system and source of redu s well as a unique protein glycyl radical site. A possible ev ionship between early deoxyribonucleotide metabolism and pri netabolism is suggested.

cleotide reductases (RNRs) are es- enzymes for all life, constituting the novo catalytic path for the produc- the deoxyribonucleotides required

generate a stable tyro R2 subunit through a O_2 by a dinuclear iro is most likely transfe

Article No. jmbi.1999.2701 available online at http

JMB

The Crystal Structure o *eutrophus* Reveals a N β-Barrel Formed by β-S

Sissel Hansen[1], Valentina Bur Kjell Andersen[2]

[1]*Protein Crystallography Group, Department of Chemistry, Faculty of Science University of Tromsø N-9037 Tromsø, Norway*

[2]*Laboratory of Microbial Gene Technology, IBF The Agricultural University of Norway, N-1432 Ås, Norway*

beam were

Ribulose-1,5- photosynthe dioxide. The leading to lo photosynthe sively, and a cally efficie groups, "gre CO_2 and O_2 like rubisco

Publications relate to all work carried out at SNBL, not just experiments from either Norwegian or Swiss scientists.

The CD-ROM affixed inside the back cover of this report contains a full bibliography for the years since 1995 as well as copies of the first page of every publication.

Cerny, R., *Powder Pattern Decomposition with the Aid of Preferred Orientation - Experimental Test.* Mat. Science Forum **321-324**, 22-27 (2000)

Cerny, R., Joubert, J.M., Latroche, M., Percheron-Gugan, A., Yvon, K., *Anisotropic diffraction peak broadening and dislocation substructure in hydrogen-cycled LANI5 and substitutional derivatives.* J. Appl. Crystl. **33**, 997-1005 (2000)

Choinowski, T., Hauser, H., Piontek, K., *Structure of Sterol carrier protein 2 at 1.8 a resolution reveals a hydrophobic tunnel suitable for lipid binding*. Biochemistry. **39**, 1897-1902 (2000)

Dalconi, M.C., Cruciani, G., Alberti, A. Ciambelli, P., Rapacciuolo, *Ni2+ ion sites in hydrated and dehydrated forms of Ni-exchanged zeolite ferrierite.* Microporous & mesoporous materials **39**, 423-430 (2000)

Dubrovinskaia.N.A. Vennstroem. M., Abrikosov. I.A., Ahuja. R., Ravindran, P. Andersson, Y., Eriksson, O., Dmitriev, V. Dubrovinsky, S. *Absence of pressure-induced structural phase transition in TI3Al up to 25 GPa*. Physical Review B, **63**, 24106 (2000)

Esterman, M.A., Lemster, K., Haibach, T, Steurer, W. *Towards the real structure of quasicrystals and approximants by analysing diffuse scattering and deconvolving the Patterson*, Z. Kristallogr. **215,** 584-596 (2000)

Fauth, F., Broennimann, C, Auderset, H. Maehlum, G., Pattison, P., Patterson, B. *Towards Microstrip Detectors for Synchrotron Powder Diffraction Facilities*, Nuclear Instrum.& Methods in Physics Research **A 439**, 138-146 (2000)

Haibach, T., Cervellino, A., Estermann, M.A., Steurer, W., *X-ray structure determination of quasicrystals - limits and potentiality*. Z. Kristallogr. **215**, 569-583 (2000)

Haibach, T., Estermann, M.A., Cervellino, A., Steurer, W. *Phase transitions in quasicrystals - the example of decagonal Al-Co-Ni.* Mat. Science & Engineering **294-296** 17-22 (2000)

Jackson, W.J., Moen, A., Nicholson, B.K., Nicholson, D.G., Porter, K.A., *An x-ray absorption spectroscopic study at the mercury Lm edge on phenylmercury (II) oxygen species*, J. Chem. Soc, Dalton Trans., **2000**, 491-498 (2000)

Kongshaug, K.O., Fjellvag, H., Lillerud, K.P., *Synthesis and characterization of a novel layered zinc phosphate.* Solid State Sciences **2,** 569-576 (2000)

Larochelle, C.L., Omary, M.A., Patterson H.H., Fischer, P., Fauth, F., Allenspach, P., Lucas, B., Pattison, P., *Optical, synchrotron x-ray and neutron diffraction investigations of structural changes in the layered compound K2Na[Ag(CN)2]3.*, Solid State Commu-nication **114**, 155-160 (2000)

Leiros, I., Hough, E., D'Arrigo, P., Carrea, G., Pedrocchi-Fantoni, G.Secundo, F., Servi. S. *Crystallization and preliminary x-ray diffraction studies of phospholipase D from streptomyces sp*. Acta. Cryst. **D56**, 466-468, (2000)

Leiros, I., Secundo, F., Zambonelli, C.Servi, S., Hough, E., *The first crystal structure of a phospholipase D*. Structure **2000,** 655-667 (2000)

Madsen, D., Pattison, P. *N-Methyl-DL-aspartic acid monohydrate*. Acta Cryst. **C56**, 1157-1158, (2000)

Maeda, K., Tuel, A., Caldarelli, S., Baerlocher, Ch. *Synthesis , structure determination and characterization of APDAB200, a new aluminosphosphate prepared with 1,4-diaminobutane*. Microporous & Mesoporous Materials **39**, 465-476 (2000)

Margadonna, S., Aslanis, E., Orassudes, K., Fitch A., Hansen, T.C., *Crystal structure of superconducting K3Ba3C60: a combined synchrotron X-ray and neutron diffraction study.* Chemistry of Materials. **12**, 2736-2740 (2000)

Marturano, P., Drozdova, L., Kogelbauer, A., Rins, R. *Fe/ZSM-5 prepared by sublimation of FeCl3: the structure of the Fe species as determined by IR, 27Al MAS NMR, and EXAFS spectroscopy.* J. of Catalysis **192**, 236-247 (2000)

Milanesio, M., Lamberti, C., Aiello, R., Testa, F., Piana, M., Viterbo, D. *Iron Location in Fe-Silicalites by Synchrotron Radiation Single Crystal X-ray diffraction.* J. Phys. Chem **B 104**, 9951-9953 (2000)

Mittl, R.E.,Deillo, C., Sargent, D., Liu, N., Klauser, S., Thomas, R.M., Gutte, B., Grueter, M.G. *The retro-GCN4 leucine zipper sequence forms a stable three-dimensional structure.* Proc.Nat.Acad.Sci, **97**, 2562-2566, (2000)

Nicholson, D.G., Nilsen, M.H. *An x-ray absorption spectroscopic study on the local environment of copper in CuAPO-5.* J.Mater.chem **10**, 1965-1971 (2000)

Oefner, C., D'Arcy, A., Henning, M., Winkler, F.K., Dale, G.E. *Structure of Human neutral endopeptidase (Neprilysin) complexed with phosphoramidon.* J. Mol. Biol. **296**, 341-349 (2000)

Olafsen, A. Fjellvag, H., Hauback, B.C. *Crystal Structure and Properties of* $Nd_4CO_3O_{10}$ Journal of Solid State Chemistry **151**, 46-55 (2000)

Onoda,M., Wada, H., Pattison, P., Yamamoto, A., Ishii, M., Chapuis, G. *Low-temperature Form (Phase II) of Ionic Conductor Ag7TaS6 Analyzed using High-Resolution Synchrotron X-Ray Powder Diffraction Data.*, Mol. Cryst. And Liq. Cryst., **341**, 75-80 (2000)

Pattison, P, Knudsen, K.D., Cerny, R., Koller, E. *Rapid characterization of complex structural phase transitions using powder diffraction and an area detector*. J. Synchrotron Rad**. 7**, 251-256 (2000)

Pattison, P, Knudsen, K.D., Fitch, A.N., *Accuracy of molecular structures determined from high-resolution powder diffraction. The example of m-fluorobenzoic acid.* J.Appl.Cryst. **33**, 82-86 (2000)

Prassides, K., Brown, CM., Margadonna, S., Kordatos, K., Tanigaki, K., Suard, E., Dianoux, AJ., Knudsen, KD. *Powder diffraction and inelastic neutron scattering studies of the Na2RbC60 fulleride.* J. Materials Chemistry, **10**, 1443-1449 (2000)

Reeuwijk, S.J., van Puig-Molina, A., Graafsma, H. *Electric-field-induced structural changes in deuterated potassium dihydrogen phosphate.*, Physical Review **B 62**, 6192-6197 (2000)

Roessli, B., Staub, U., Amato, A., Herlach, D., Pattison, P., Sablina, K., Petrakovskii, G.A. *Magnetic Phase Transitions in the double spin-chains compound LiCu2O2*. Physica B to be published

Scheidegger, S., Estermann, M.E., Steurer, W. *Correction of specimen absorption in x-ray diffuse scattering experiments with area-detector systems.* J.Appl.Cryst. **33**, 35-48 (2000)

Sobalik, Z., Dedecek, J., Kaucky, D., Wichterlova, B., Drozdova, L., Prins, R. *Structure, distribution, and properties of Co Ions in ferrierite revealed by FTIR, UV-Vis, and EXAFS*. J. of Catalysis **194**, 330-342 (2000)

Thorkildsen, G., Larsen, H.B., Mathiesen, R.H., Mo.F. *Three-beam interference measurements with a six-circle k difractometer* J.Appl.Cryst. **33**, 49-51 (2000)

Tuel, A., Caldarelli, S., Meden, A., McCusker, L.B., Baerlocher, C., Ristic, A., Rajic, N., Mali, G. *NMR Characterization and Rietveld refinement of the structure of rehydrated AlPO4-34.* J. Phys. Chem. **B 104**, 5697-5705 (2000)

THE SWISS - NORWEGIAN BEAMLINES AT ESRF

AN ADVANCED FACILITY FOR THE SOLUTION OF COMPLEX CRYSTALLOGRAPHIC PROBLEMS